Defining Material Parameters in Commercial EM Solvers for Arbitrary Metal-Based THz Structures

Elpida Episkopou, *Student Member, IEEE*, Stergios Papantonis, *Student Member, IEEE*, William J. Otter, *Student Member, IEEE*, and Stepan Lucyszyn, *Senior Member, IEEE*

***Abstract*—Frequency-domain solvers are used extensively for modeling arbitrary metal-based terahertz structures. Four well-known commercially available electromagnetic (EM) modeling software packages include HFSS™, CST Microwave Studio®, EMPro, and RSoft. However, there are a number of operational issues that relate to how they can be used to obtain more meaningful and accurate results. Even experienced users of these and similar software packages may not fully appreciate some of the subtle ambiguities in defining boundaries and material parameters for use in THz applications. To this end, a detailed comparative study has been undertaken, in consultation with all four vendors. First, in order to avoid introducing ambiguities, frequency dispersion in materials has to be clearly defined from first principles; in both intrinsic and effective forms. Different frequency dispersion models are then introduced for 'metal-like' materials. To act as benchmark structures, conventional air-filled metal-pipe rectangular waveguides, associated cavity resonators and a spoof surface plasmon waveguide have been simulated, using a raft of different approaches; with a view to illustrating quantifiable weaknesses in commercial software packages for simulating arbitrary metal-based THz structures. This paper highlights intuitive and logical approaches that give incorrect results and, where possible, makes recommendations for the most appropriate solutions that have hitherto not been given in Technical Notes.**

***Index Terms*—Cavity resonators, commercial software, frequency domain, metal, numerical modeling, terahertz (THz), waveguides.**

I. Introduction

OVER the past two decades, there has been increasing interest in the 0.3 to 10 THz frequency range for a variety of applications. Currently, the "THz gap" is used for highly specialized applications (e.g., radiometric imaging and spectroscopy). However, in order to fully exploit this part of the frequency spectrum and, thus, open up the "THz gap" to ubiquitous applications, there will be increasing reliance on the use of commercial electromagnetic (EM) modeling software (e.g., HFSS™ [1]–[9], CST Microwave Studio® [8]–[11] and RSoft [12]–[17]) to predict the performance of metal-based terahertz structures. Moreover, in the 0.3–10 THz frequency range, dispersion in the conductivity of metal-based structures can affect results significantly and, therefore, has to be properly taken into account when passive components are modeled.

While commercially available software packages can generally predict the actual performance of arbitrary 3D structures, the correct approach to selecting the most appropriate boundary conditions, defining a material's parameters and being able to enter its real or complex values within the software are not always straightforward [18]. With no or limited and ambiguous information given in Technical Notes, the wrong approach may result in significant errors. Indeed, it has been found that some intuitive and logical approaches yield incorrect results, which may not be apparent to even experienced EM software users [19]–[21].

First, relevant background theory for assigning material parameters for frequency dispersive media is given. This is necessary in order to avoid introducing ambiguities and errors. This paper then investigates various frequency-domain approaches to modeling benchmark metal-based THz structures, using four well-known software packages: Ansys' High Frequency Structure Simulator (HFSS™),[1] CST Microwave Studio® (CST MWS),[2] Agilent's newly released Electromagnetic Professional (EMPro),[3] and RSoft.[4]

With few detailed measurements of passive metal-based structures, operating within the "THz gap," being reported in the open literature [22], the classical relaxation-effect (or Drude dispersion) model has been adopted as reference. This phenomenological analytical model has previously been shown to fit accurate room temperature measurements in the lower terahertz range [22], unlike more empirical models [23].

Here, classical air-filled metal-pipe rectangular waveguides (MPRWGs) and associated cavity resonators are used as benchmark structures to represent the millimeter-wave community moving up in frequency into the "THz gap"; while spoof (or designer) surface plasmon waveguides represent the optics community moving down in frequency into the "THz gap."

Within HFSS™, its frequency-domain solver employs the finite-element method (FEM), with its ability to handle complex geometries efficiently; while within CST MWS, high frequency 3D EM field simulation can be performed using the frequency-domain solver based on the finite integration technique (FIT). Within EMPro, its frequency-domain solver employs FEM; while within RSoft, its FemSIM is a generalized

Manuscript received March 20, 2012; accepted July 09, 2012. Date of publication August 24, 2012; date of current version August 30, 2012. This work was supported by the Engineering and Physical Sciences Research Council (EPSRC), U.K., under Platform Grant EP/E063500/1 and the Val O'Donoghue Scholarship.

The authors are with the Centre for Terahertz Science and Engineering, Imperial College London, Exhibition Road, London SW7 2AZ, U.K. (e-mail: e.episkopou10@imperial.ac.uk; s.papantonis10@imperial.ac.uk; william.otter06@imperial.ac.uk; s.lucyszyn@imperial.ac.uk).

Color versions of one or more of the figures in this paper are available online at http://ieeexplore.ieee.org.

Digital Object Identifier 10.1109/TTHZ.2012.2208456

[1][Online]. Available: http://www.ansoft.com/products/hf/hfss/

[2][Online]. Available: http://www.cst.com/

[3][Online]. Available: http://www.home.agilent.com/agilent

[4][Online]. Available: http://www.rsoftdesign.com

mode solver based on FEM, which can calculate transverse and cavity modes of any 1D or 2D cross section. In consultation with all four associated vendors, all possible modeling strategies have been investigated in depth and, for the first time, detailed recommendations for the most appropriate solutions are given that have hitherto not been given in Technical Notes.

II. Frequency Dispersion in Materials

A. Intrinsic and Effective Material Parameters

It will be seen later that one of the main issues associated with inaccurate modeling is related to ambiguities introduced during material parameter definition. For this reason, it is first necessary to reproduce textbook theory that underpins frequency-domain solvers. The relevant background to defining material parameters for frequency dispersive media starts with the generalized Ampere's law (with the associated variables having their usual meaning)

$$\nabla \times \boldsymbol{H} = \boldsymbol{J}_f + \frac{\partial \boldsymbol{D}}{\partial t} \tag{1}$$

where $\boldsymbol{J}_f = \boldsymbol{J}_i + \boldsymbol{J}_c$. Assuming that the impressed (external) current density $\boldsymbol{J}_i$ is zero, the free current density $\boldsymbol{J}_f$ reduces to the conduction current density $\boldsymbol{J}_c$. For an isotropic, linear and dispersive medium the constitutive equations can be written using a Taylor series as

$$\boldsymbol{D} = \varepsilon \boldsymbol{E} + \varepsilon_1 \frac{\partial \boldsymbol{E}}{\partial t} + \varepsilon_2 \frac{\partial^2 \boldsymbol{E}}{\partial t^2} + \varepsilon_3 \frac{\partial^3 \boldsymbol{E}}{\partial t^3} + \cdots \tag{2}$$

$$\boldsymbol{B} = \mu \boldsymbol{H} + \mu_1 \frac{\partial \boldsymbol{H}}{\partial t} + \mu_2 \frac{\partial^2 \boldsymbol{H}}{\partial t^2} + \mu_3 \frac{\partial^3 \boldsymbol{H}}{\partial t^3} + \cdots \tag{3}$$

$$\boldsymbol{J} = \sigma \boldsymbol{E} + \sigma_1 \frac{\partial \boldsymbol{E}}{\partial t} + \sigma_2 \frac{\partial^2 \boldsymbol{E}}{\partial t^2} + \sigma_3 \frac{\partial^3 \boldsymbol{E}}{\partial t^3} + \cdots \tag{4}$$

where ε_q, μ_q, and σ_q are weighting factors for the higher order terms. Now, (1)–(4) can be expressed for the steady-state frequency domain (with $e^{+j\omega t}$ time harmonic dependence, where the complex operator $j = \sqrt{-1}$ and $\omega = \text{angular frequency}$) as follows:

$$\nabla \times \boldsymbol{H} = \boldsymbol{J}_f + j\omega \boldsymbol{D} \tag{5}$$

$$\begin{aligned} \boldsymbol{D} &= \varepsilon \boldsymbol{E} + j\omega\varepsilon_1 \boldsymbol{E} - \omega^2 \varepsilon_2 \boldsymbol{E} - j\omega^3 \varepsilon_3 \boldsymbol{E} + \cdots \\ &\equiv \left(\underbrace{\varepsilon'(\omega) - j\varepsilon''(\omega)}_{\varepsilon(\omega)} \right) \boldsymbol{E} \end{aligned} \tag{6}$$

$$\begin{aligned} \boldsymbol{B} &= \mu \boldsymbol{H} + j\omega\mu_1 \boldsymbol{H} - \omega^2 \mu_2 \boldsymbol{H} - j\omega^3 \mu_3 \boldsymbol{H} + \cdots \\ &\equiv \left(\underbrace{\mu'(\omega) - j\mu''(\omega)}_{\mu(\omega)} \right) \boldsymbol{H} \end{aligned} \tag{7}$$

$$\begin{aligned} \boldsymbol{J}_c &= \sigma \boldsymbol{E} + j\omega\sigma_1 \boldsymbol{E} - \omega^2 \sigma_2 \boldsymbol{E} - j\omega^3 \sigma_3 \boldsymbol{E} + \cdots \\ &\equiv \left(\underbrace{\sigma'(\omega) - j\sigma''(\omega)}_{\sigma(\omega)} \right) \boldsymbol{E} \end{aligned} \tag{8}$$

where $\varepsilon(\omega)$, $\mu(\omega)$, and $\sigma(\omega)$ describe the intrinsic bulk effects of polarization, magnetization and conductivity, in complex notation form, respectively. It is worth mentioning that: with normal metals at room temperature $\varepsilon(\omega) \cong \varepsilon_o$, the permittivity of free space; with non-magnetic materials $\mu(\omega) = \mu_o$, the permeability of free space; and with low frequency room temperature modeling of materials $\sigma(\omega) \cong \sigma_o$, intrinsic bulk conductivity at dc. In the more general case, (5)–(8) yield the following:

$$\begin{aligned} \nabla \times \boldsymbol{H} &= \boldsymbol{J}_c + j\omega \boldsymbol{D} \\ &= \left(\underbrace{\sigma(\omega) + j\omega\varepsilon(\omega)}_{\sigma_{\text{eff}}(\omega)} \right) \boldsymbol{E} \\ &= j\omega \left(\underbrace{\varepsilon(\omega) - j\frac{\sigma(\omega)}{\omega}}_{\varepsilon_{\text{eff}}(\omega)} \right) \boldsymbol{E}. \end{aligned} \tag{9}$$

From (9), it is obvious that the effective parameters $\sigma_{\text{eff}}(\omega)$ and $\varepsilon_{\text{eff}}(\omega)$ can be used interchangeably; being related to each other by the textbook expression:

$$\sigma_{\text{eff}}(\omega) = j\omega\varepsilon_{\text{eff}}(\omega) \tag{10}$$

where the effective permittivity $\varepsilon_{\text{eff}}(\omega) = \varepsilon_o \varepsilon_{r,eff}(\omega)$ and $\varepsilon_{r,eff}(\omega)$ is the relative effective permittivity (also referred to as the dielectric function; although, this should not be confused with the dielectric constant, which represents only the real part of the relative effective permittivity).

Now, partitioning (9) into its real and imaginary parts, the following is obtained:

$$\begin{aligned} \nabla \times \boldsymbol{H} &= \left[\left(\underbrace{\sigma'(\omega) + \omega\varepsilon''(\omega)}_{\sigma'_{\text{eff}}(\omega)} \right) - j \left(\underbrace{\sigma''(\omega) - \omega\varepsilon'(\omega)}_{\sigma''_{\text{eff}}(\omega)} \right) \right] \boldsymbol{E} \\ &= j\omega \left[\left(\underbrace{\varepsilon'(\omega) - \frac{\sigma''(\omega)}{\omega}}_{\varepsilon'_{\text{eff}}(\omega)} \right) - j \left(\underbrace{\varepsilon''(\omega) + \frac{\sigma'(\omega)}{\omega}}_{\varepsilon''_{\text{eff}}(\omega)} \right) \right] \boldsymbol{E}. \end{aligned} \tag{11}$$

By rearranging (11) for $\varepsilon_{\text{eff}}(\omega)$ the effective dielectric loss tangent $\tan\delta_e(\omega)$ is defined (even for a metal [24]) as follows:

$$\begin{aligned} \varepsilon_{\text{eff}}(\omega) &= \varepsilon'_{\text{eff}}(\omega)(1 - j\tan\delta_e(\omega)) \\ \text{where} \quad \tan\delta_e(\omega) &\equiv \frac{\varepsilon''_{\text{eff}}(\omega)}{\varepsilon'_{\text{eff}}(\omega)} = \frac{\varepsilon''_{r,\text{eff}}(\omega)}{\varepsilon'_{r,eff}(\omega)} = \frac{\sigma'_{\text{eff}}(\omega)}{\sigma''_{\text{eff}}(\omega)}. \end{aligned} \tag{12}$$

As can be seen from (12), the dielectric loss tangent quantifies the losses for a non-magnetic material but it does not distinguish the origins of different loss mechanisms. In other words, it does not give any information about the polarization or conductivity loss contributions separately. This means that when material parameters are being evaluated experimentally the effective parameters [including $\tan\delta_e(\omega)$]) should be used. However, in the open literature, many authors loosely use the terminology "*complex permittivity*" or "*complex conductivity*" to describe the effective parameters, based on the fact that the effective parameters are complex numbers [25]–[29]. This can be confusing if not defined explicitly, since the intrinsic permittivity and conductivity themselves can be complex numbers. Thus, it may be ambiguous as to whether the authors are referring to the intrinsic

parameters $\varepsilon(\omega)$, $\sigma(\omega)$ or to their associated effective parameters $\varepsilon_{\text{eff}}(\omega)$, $\sigma_{\text{eff}}(\omega)$—with the latter set always being complex numbers, even when the former are represented by purely real quantities. For example, in the case where frequency dispersion of polarization can be neglected (e.g., metals having $\varepsilon'(\omega) \cong \varepsilon_o$ and $\varepsilon''(\omega) = 0$):

$$\varepsilon_{\text{eff}}(\omega) = \left(\varepsilon'(\omega) - \frac{\sigma''(\omega)}{\omega}\right) - j\left(\frac{\sigma'(\omega)}{\omega}\right) \tag{13}$$

$$\tan\delta_e(\omega) = \frac{\sigma'(\omega)}{\omega\varepsilon'(\omega) - \sigma''(\omega)}. \tag{14}$$

To this end, (6)–(8) must always be compatible with the principle of conservation of energy, which in electromagnetic systems can be expressed by Poynting's theorem. Also, the passivity of such materials implies that the power dissipated per cycle per unit volume must be non-negative. Thus

$$\Re\left\{\frac{1}{2}\,\boldsymbol{E}\cdot\boldsymbol{J}_c^* + \frac{j\omega}{2}(\boldsymbol{B}\cdot\boldsymbol{H}^* - \boldsymbol{E}\cdot\boldsymbol{D}^*)\right\} \geq 0 \tag{15}$$

with the equality only being valid for a lossless material. Substituting (6)–(8) into (15) and rewriting in quadratic form gives (16), shown at the bottom of the page. Using the general relationship:

$$\Re\{\boldsymbol{A}^*\cdot\boldsymbol{M}\cdot\boldsymbol{A}\} = \boldsymbol{A}^*\cdot\boldsymbol{M}'\cdot\boldsymbol{A}, \qquad \text{where } \boldsymbol{M}' = \frac{\boldsymbol{M}+\boldsymbol{M}^\dagger}{2} \tag{17}$$

where † represents the conjugate transpose matrix and taking into account that (16) holds for arbitrary electric and magnetic fields, the matrix $\boldsymbol{M}'$ must be positive semi-definite. This is ensured by the following two conditions:

$$\sigma'_{\text{eff}}(\omega) = (\sigma'(\omega) + \omega\varepsilon''(\omega)) \geq 0 \tag{18}$$

$$\mu''(\omega) \geq 0. \tag{19}$$

In order that (18) holds for arbitrary frequencies, the conditions $\sigma'(\omega) \geq 0$ and $\varepsilon''(\omega) \geq 0$ have to be verified.

When the classical relaxation-effect model for normal metals at room temperature is used, the intrinsic bulk conductivity is given by the following expression [20], [24]:

$$\sigma(\omega) = \frac{\sigma_o}{1+j\omega\tau} = \left(\underbrace{\frac{\sigma_o}{1+\omega^2\tau^2}}_{\sigma'(\omega)}\right) - j\left(\underbrace{\frac{\sigma_o\omega\tau}{1+\omega^2\tau^2}}_{\sigma''(\omega)}\right) \tag{20}$$

where τ is the phenomenological scattering relaxation time (also referred to as the collision time by HFSS™, and CST MWS) and both $\sigma'(\omega)$ and $\sigma''(\omega)$ are always positive numbers.

It is important to note that if a time dependence of the form $e^{-j\omega t}$ is used, the complex operator "$+j$" in all the previous equations must be replaced with "$-j$", resulting in material parameters being redefined by the forms $\varepsilon(\omega) = \varepsilon'(\omega) + j\varepsilon''(\omega)$, $\mu(\omega) = \mu'(\omega) + j\mu''(\omega)$, $\sigma(\omega) = \sigma'(\omega) + j\sigma''(\omega)$ and $\sigma_{\text{eff}}(\omega) = -j\omega\varepsilon_{\text{eff}}(\omega) = \sigma(\omega) - j\omega\varepsilon(\omega)$. While this point may seem obvious, errors will be introduced when parameters and equations that adopt different conventions (e.g., when originating from different sources) are inadvertently mixed during the modeling process. By default, HFSS™, CST MWS, and EMPro adopt the $e^{+j\omega t}$ convention; while RSoft adopts the $e^{-j\omega t}$ convention.

B. Frequency Dispersion in Metals

Equation (20) represents the classical relaxation-effect model for describing the frequency-temperature dispersion due to free carriers within a normal material; while the simple relaxation-effect model and the classical skin-effect model are derived by taking into account only the real part of intrinsic bulk conductivity $\sigma'(\omega)$ and σ_o, respectively [20], [24]. For a generic material, its intrinsic impedance η (e.g., representing the surface impedance Z_s of a metal) is given by the following textbook expression:

$$\eta = \sqrt{\frac{\mu(\omega)}{\varepsilon_{\text{eff}}(\omega)}} = \sqrt{\frac{j\omega\mu(\omega)}{\sigma_{\text{eff}}(\omega)}} = \sqrt{\frac{j\omega\mu(\omega)}{\sigma(\omega)+j\omega\varepsilon(\omega)}} \equiv Z_s. \tag{21}$$

With normal materials, one can neglect the dispersion effects in magnetization, so that $\mu'(\omega) = \mu_o\mu'_r$ and $\mu''(\omega) = 0$ (while at terahertz frequencies $\mu'_r \sim 1$) [30] and assuming a metal with sufficiently high conductivity so that the displacement current term can be neglected $\sigma_{\text{eff}}(\omega) \cong \sigma(\omega)$)

$$Z_s = R_s + jX_s \cong \sqrt{\frac{j\omega\mu_o\mu'_r}{\sigma(\omega)}}. \tag{22}$$

For the three aforementioned frequency dispersion models, (22) can be expanded out using the following expressions for the surface resistance and reactance [20], [24]:

Classical relaxation-effect (or Drude dispersion) model

$$R_s = R_{so}\sqrt{\sqrt{1+(\omega\tau)^2}-\omega\tau} = X_s\left(\sqrt{1+(\omega\tau)^2}-\omega\tau\right)$$
$$X_s = R_{so}\sqrt{\sqrt{1+(\omega\tau)^2}+\omega\tau} = R_s\left(\sqrt{1+(\omega\tau)^2}+\omega\tau\right). \tag{23}$$

Simple relaxation-effect model

$$R_s = R_{so}\sqrt{1+(\omega\tau)^2} \text{ and } X_s = R_s. \tag{24}$$

Classical skin-effect model

$$R_s = R_{so} = \sqrt{\frac{\omega\mu_o\mu'_r}{2\sigma_o}} \text{ and } X_s = R_s. \tag{25}$$

$$\Re\left\{\begin{bmatrix}\boldsymbol{E}^* & \boldsymbol{H}^*\end{bmatrix}\begin{bmatrix}(\sigma'(\omega)+\omega\varepsilon''(\omega)) + j(\sigma''(\omega)-\omega\varepsilon'(\omega)) & 0\\ 0 & j\omega(\mu'(\omega)-j\mu''(\omega))\end{bmatrix}\begin{bmatrix}\boldsymbol{E}\\ \boldsymbol{H}\end{bmatrix}\right\} \geq 0. \tag{16}$$

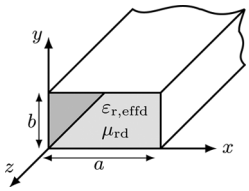

Fig. 1. Uniform dielectric-filled MPRWG benchmark structure.

III. THz Metal-Pipe Rectangular Waveguide Modeling

Metal-pipe rectangular waveguides and associated cavity resonators are simulated at THz frequencies, where frequency dispersion in conductivity has previously been found to affect predicted results [20], [31]. A MPRWG with internal dimensions $a \times b = 100 \times 50$ μm^2 (i.e., JPL-100 standard [20], [32]), with gold walls having room-temperature parameter values of $\sigma_o = 4.517 \cdot 10^7$ S/m, $\tau = 27.135$ fs and $\mu'_r = 0.99996$ [22], was used as a benchmark structure, as illustrated in Fig. 1.

To simplify the analysis, this waveguide is assumed to operate in the fundamental TE_{10} mode, so that closed-form analytical expressions can be used for direct comparison with the numerical simulation results. For example, the propagation constants γ_{mn} for a MPRWG supporting $\mathrm{TE}_{\mathrm{mn}}$ modes can be calculated using the variational method [33], which can be expressed in the simpler form for $\mathrm{TE}_{\mathrm{mo}}$ modes as follows [34]:

$$\gamma_{mo}^2 = \Gamma_d^2 - j\frac{2Z_s}{\omega\mu_o\mu'_{rd}b}\left[\left(\frac{\Gamma_d m\pi}{k_{cd}a}\right)^2 - k_{cd}^2\left(1+\frac{2b}{a}\right)\right] \quad (26)$$

where

$$\begin{aligned}\Gamma_d^2 &= k_{cd}^2 - k_{od}^2\\ k_{cd} &= \omega_c\sqrt{\mu_o\mu'_{rd}\varepsilon_o\varepsilon'_{r,effd}}\\ k_{od} &= \omega\sqrt{\mu_o\mu'_{r,effd}\varepsilon_o\varepsilon'_{r,effd}(1-j\tan\delta_{ed})}\end{aligned}$$

and μ'_{rd}, $\varepsilon'_{r,effd}$, and $\tan\delta_{ed}$ are the real part of the relative permeability, dielectric constant and effective loss tangent for the dielectric filler, respectively.

In HFSS™, the classical skin-effect model is employed, by default, with σ_o being entered in the material setup dialog box. Alternatively, the simple relaxation-effect model can be used by entering a data file containing the non-complex (i.e., real notation form) conductivity values calculated *a priori* at each discrete frequency point. In order to speed up the simulation times, solid metal walls can be replaced by boundaries. Both frequency dispersion models can be used in the material parameters for a 3D "solid object" or boundary condition. With the former, the use of bulk meshing is dependent on the threshold value of conductivity (for HFSS™ this is 10^5 S/m, by default); there is no bulk meshing with any of the boundaries. It must be noted, however, that the classical relaxation-effect model cannot be used directly; while current versions of HFSS™ (e.g., up to version 13) allow complex numbers to be entered into the conductivity value field it does not actually support these complex values [20], as will be explained in greater detail.

For example, with the Finite Conductivity Boundary (FCB), complex conductivity values can be entered using the following

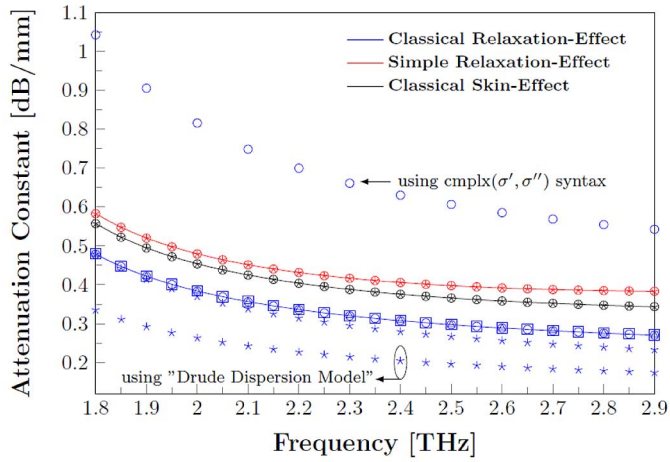

Fig. 2. Attenuation constant for the dominant TE_{10} mode with the 100 μm JPL band gold MPRWG; Lines: calculated values from analytical models using (26); Circles: simulated values using HFSS™, Stars: simulated values using CST MWS; Triangles: simulated values using EMPro; and Squares: simulated values using RSoft.

syntaxes: $\sigma' - \sigma''j$ or $\sigma' - \sigma''i$. Here, the imaginary term σ'' is simply ignored in calculations, thus giving results that coincide with the simple relaxation-effect model [20]. Alternatively, complex conductivity values can be entered using the following suggested syntax [35]: $\mathrm{cmplx}(\sigma', \sigma'')$, where $\sigma'' \geq 0$. Unfortunately, it has been found that this latter method gives incorrect results, as can be seen in Fig. 2 with the modeling of attenuation constant for a uniform air-filled MPRWG. However, with the Layered Impedance Boundary (LIB), $\varepsilon'_{r,eff}$ and σ' can be entered directly, so long as the metal's dielectric loss tangent is set to zero, yielding the correct results. It should be pointed out that when only the intrinsic conductivity is entered, as described previously with the complex notation form, the problems associated with the LIB are also the same for the FCB. Alternatively, with the Impedance Boundary (IB), the appropriate complex surface impedance Z_s can be entered directly for each discrete frequency point. In this case, as can be seen in Fig. 2 the results reported by HFSS™, are in excellent agreement with the classical relaxation-effect model with (26). It must be noted that since the complex value of surface impedance must be entered *a priori*, significant errors may result if tuning or optimization routines are employed with structures where the spectral features of interest can shift to frequencies not represented by the list of discrete frequency points that give the associated values of complex surface impedances.

The above approaches are also found in CST MWS (e.g., versions up to 2011 service pack 7), where the simple relaxation-effect and classical skin-effect models can be applied to the bulk conductivity of a solid objector Conducting Wall Boundary (CWB). However, with the simple relaxation-effect model, the conductivity values have to be entered at each discrete frequency point, since the software does not currently support a data file import for conductivity. Alternatively, one could define a "normal material" type, whose permittivity is given by the relative effective value calculated using (13) and assuming $\sigma'' = 0$, and then enter a data file containing the permittivity values as a "user defined" dispersion model. However, the results were still found to be inaccurate, probably

TABLE I
SUMMARY OF DIFFERENT MODELING STRATEGIES FOR METAL STRUCTURES USING HFSS™, AND CST MWS

		HFSS™		CST MWS	
		Eigenmode Solver	**Other solvers**	**Eigenmode Solver**	**Other solvers**
Solid object definition	**Input parameters**	σ_o or data file of $\sigma'(f)$		σ_o or data file of $\varepsilon'_{r,eff}(f)$ and $\varepsilon''_{r,eff}(f)$	σ_o or discrete points of $\sigma'(f)$ or ω_p and ω_τ
	Error	significant	negligible	significant	negligible/significant
	Model	(1) classical skin-effect (2) simple relaxation-effect (3) classical relaxation-effect*		(1) classical skin-effect (2) simple relaxation-effect (3) classical relaxation-effect	
	Comments	without "solve inside" function enabled		With (1), σ_o is ignored and PEC is assumed. Post-processing is then required. With (2) and (3), impractical resources are required	For (1) and (2) the error is negligible, for (3) the error is significant
FCB (HFSS™) and **CWB** (CST MWS)	**Input parameters**	σ_o or $\sigma'(f_1)$	σ_o or data file of $\sigma'(f)$	σ_o	σ_o or $\sigma'(f)$
	Error	negligible /small	negligible	negligible	negligible
	Model	(1) classical skin-effect (2) simple relaxation-effect			
	Comments	In general, f_1 is not known *a priori* so (2) is of limited use		Input parameters are ignored, lossy metals are considered as PEC and σ is entered in the post-processing stage	Input parameters should be entered at each discrete frequency point
LIB (HFSS™)	**Input parameters**	data file of $\varepsilon'_{r,eff}(f)$ and $\sigma'(f)$	data file of $\varepsilon'_{r,eff}(f)$ and $\sigma'(f)$		
	Error	negligible	negligible		
	Model	(1) classical skin-effect (2) simple relaxation-effect (3) classical relaxation-effect			
	Comments	In general, this is a two-run simulation			
IB (HFSS™) and **SIM** (CST MWS)	**Input parameters**	$R_s(f_1), X_s(f_1)$	$R_s(f)$, $X_s(f)$	Data file of $R_s(f), X_s(f)$	
	Error	negligible	negligible	negligible	significant
	Model	(1) classical skin-effect (2) simple relaxation-effect (3) classical relaxation-effect		(1) classical skin-effect (2) simple relaxation-effect	(1) classical skin-effect (2) simple relaxation-effect (3) classical relaxation-effect
	Comments	In general, f_1 is not known *a priori* so (2) and (3) are of limited use	Input parameters should be entered at each discrete frequency point	Input parameters are ignored, lossy metals are considered as PEC and σ is entered in the post-processing stage	

* If the 'solve inside' function is disabled the results will not be correct. However, with the 'solve inside' enabled and with the input parameters given in Table II the results should be correct; although this approach is impractical as explained in the Discussion section.

due to poor meshing inside the metal. Again, the classical relaxation-effect model cannot be used explicitly, but the "Surface Impedance" Material (SIM) type can be defined with a data file containing the complex surface impedance values at each discrete frequency point. Fortunately, CST MWS interpolates between data points and thus tuning or optimization routines can be employed, in contrast to HFSS™. Although, as can be seen in Fig. 2, the results increasingly diverge from the analytical model as frequency increases; the reason for this is unknown. Alternatively, an "ohmic sheet" material type can be used where the surface impedance is defined at each discrete frequency point. However, this approach is also found to give incorrect results.

In principle, the solid walls of the waveguide can be treated as dielectrics (i.e., a "normal material" type) by defining for the metal: $\varepsilon'_r = 1$; the angular plasma frequency $\omega_p = \sqrt{\sigma_o/\varepsilon_o\tau}$; and collision damping angular frequency $\omega_\tau = 1/\tau$ (this approach is also used in RSoft). This also gives incorrect results, as seen for the "Drude Dispersion Model" results shown in Fig. 2, probably due to poor meshing. All the above approaches for HFSS™ and CST MWS are summarized in Table I.

With EMPro (e.g., version 2011.11) frequency dispersive metals are not supported. Although there are frequency dispersion models for dielectrics, which can emulate metals by entering appropriate parameters, the losses are underestimated because of inadequate mesh densities inside the metal. Thus, the only way to obtain accurate results is by using a non-dispersive "Surface Resistance" (SR) material type, which actually corresponds to the real and imaginary parts of the surface impedance, entered at each discrete frequency point (as with the IB in HFSS™). In other words, iterative simulations have to be reassigned with new values for surface impedance at

every frequency point. In the current version of EMPro, the thickness in the material setup window must be set to zero, for correct results, otherwise the losses reported are greater than expected and these losses increase with increasing thickness. Alternatively, the intrinsic bulk dc conductivity σ_o of the material can be entered, giving results that coincide with the classical skin-effect model.

Finally, with RSoft, standard linear dispersion models can be used by entering their characteristic parameters ω_p and $\omega_\tau = 1/\tau$ for the metal, producing results that are in excellent agreement with the classical relaxation-effect model.

IV. THz Cavity Resonator Modeling

Simple rectangular waveguide cavity resonators, operating in the dominant TE_{101} mode, have also been simulated using eigenmode solvers that predict the complex eigenmode frequencies $\tilde{\omega}_0 = \omega_0' + j\omega_0''$. With a nonzero surface reactance X_s, due to contributions from both the classical skin-effect and kinetic surface inductances [24], the lossless (or driven) resonant angular frequency $\omega_0 = |\tilde{\omega}_0|$ of the cavity is reduced from the ideal resonant angular frequency ω_I. Furthermore, a nonzero surface resistance R_s, due to ohmic losses, results in further frequency detuning; shifting the natural resonant angular frequency down from ω_0 to the damped (or undriven) resonant angular frequency ω_0'. Thus, the overall level of natural frequency detuning is $\Delta\omega_0' = (\omega_I - \omega_0')$ [20].

In summary, at terahertz frequencies, when compared to the classical relaxation-effect model [20], [24]: the classical skin-effect model overestimates the surface resistance (i.e., inflating losses) and underestimates surface reactance (i.e., undervaluing frequency detuning); the simple relaxation-effect model gives reasonably good predictions for detuning, but greatly inflates losses.

Assuming losses are small enough, one can use the well-known expressions, derived using perturbation theory [20], [36], for calculating the lossless resonant frequency and the unloaded quality factor at this frequency. Solving (27) for the lossless resonant frequency ω_0 [20], and from (28) the corresponding unloaded quality factor, can be easily obtained

$$X_s(\omega_0) - 2\Gamma(\omega_I - \omega_0) \cong 0 \tag{27}$$

$$R_s(\omega_0) = \frac{\omega_0\Gamma}{Q_u(\omega_0)} \approx \frac{\omega_I\Gamma}{Q_u(\omega_0).} \tag{28}$$

For the TE_{101} mode, Γ represents the geometrical factor given by the textbook expression:

$$\Gamma = \mu_0 \left(\frac{abd(a^2+d^2)}{2[2b(a^3+d^3)+ad(a^2+d^2)]} \right) \quad [\mathrm{H}]. \tag{29}$$

It should be noted that both HFSS™ and CST MWS use frequency $f = \omega/2\pi$, rather than angular frequency ω, when entering parameters or displaying results, unless explicitly stated (e.g., plasma angular frequency in CST MWS).

The simulated and calculated values for the unloaded Q-factor $Q_u(f_0)$ and the overall frequency detuning $(f_\mathrm{I} - f_0')$ are plotted in Fig. 3, for a variety of gold rectangular cavities having respective internal width, height and length dimensions of $a \times b \times d = a \times a/2 \times \sqrt{2}a$ [20]. With the classical skin-effect model, without and with the displacement current term, respectively, both the FCB and LIB can be used by entering σ_o.

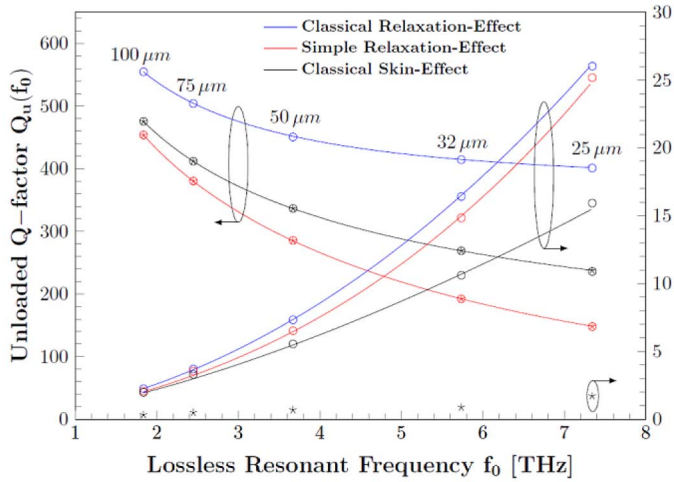

Fig. 3. Unloaded Q-factor $Q_u(f_0)$ and overall frequency detuning $(f_\mathrm{I} - f_0')$ for the TE_{101} mode gold cavity resonators for different cavity width dimensions a; Lines: calculated values from analytical models (27–29, 33); Circles: simulated values using HFSS™; Stars: simulated values using CST MWS (almost identical results for frequency detuning with both simple relaxation-effect and classical skin-effect models).

However, for the simple and classical relaxation-effect models, the user must follow one of the approaches outlined below.

A. HFSS™ With FCB and IB

With the simple relaxation-effect model, the FCB and IB can be used by entering the conductivity $\sigma'(f_\mathrm{I})$ and complex surface impedance $Z_s(f_\mathrm{I})$ values, respectively, with values calculated at the ideal resonant frequency f_I. As can be seen in Fig. 3, the convenient choice of using the ideal resonant frequency gives a reasonably good approximation, in terms of predicting the amount of frequency detuning $(f_\mathrm{I} - f_0')$ and unloaded quality factor $Q_u(f_0)$.

Note that, in HFSS™, the unloaded Q-factor is calculated with the assumption that the eigenfrequency of a mode can be represented by the complex resonant frequency of a lumped-element *RLC* resonator, i.e., defined by the following [36]:

$$Q_u(f_0) = \frac{f_0}{2f_0''} \tag{30}$$

where $f_0 = |\tilde{f}_0|$ and $\tilde{f}_0 = f_0' + jf_0''$. It will be seen that (30) is inherently sensitive to errors in the complex resonant frequency $\tilde{f}_0$ and, in particular, f_0''.

With the classical relaxation-effect model, the FCB cannot be used (as it does not support complex conductivity values). However, by entering $Z_s(f_\mathrm{I})$, the IB can give excellent results when frequency detuning is not too large.

For this benchmark structure, given its simple geometrical shape, the ideal resonant frequency can be easily calculated for large conductivities. However, with a more complicated geometrical structure, it may not be possible to predict the ideal resonant frequencies for each and every mode and so this approach cannot be used to give accurate results.

B. HFSS™ With LIB

With the LIB, unlike with the FCB, the eigenmode solver supports frequency-dependent material parameters and can be used for arbitrary structures without *a priori* knowledge of the ideal

resonant frequency. However, for accurate results, the starting frequency that the user enters during setup has to be very close to the real part of the complex eigenfrequency f_0' (but lower than f_0', so that the solver does not skip the mode of interest) in order for the software to accurately calculate f_0''. Otherwise, the results may contain significant errors in both f_0'' and unloaded quality factor $Q_u(f_0)$ calculated using (30). Unfortunately, the resonant frequency f_0 of an arbitrary structure is not known *a priori*.

To overcome this problem, one needs to simulate the structure using a single iteration, where the starting frequency in the iteration is very close (but lower) than the real part of the resonant frequency generated by the initial simulation. This is necessary in order for the software to accurately calculate f_0'' and, hence, $Q_u(f_0)$.

Alternatively, when the ideal resonant frequency $f_{\rm I}$ and unloaded Q-factor $Q_u(f_{\rm I})$ are of most interest, rather than the damped resonant frequency f_0', it has been found that one can avoid the iterative simulation, without *a priori* knowledge of the resonant frequency, by having the starting frequency f_s well below resonance (i.e., $f_s \ll f_0'$). The damped resonant frequency obtained with this approach tends to the ideal resonant frequency (the lower the starting frequency the closer $f_0' \rightarrow f_{\rm I}$). However, f_0'' and, hence, $Q_u(f_0)$ using (30) will be completely incorrect. Therefore, instead of using (30), the fields calculator can be employed to compute the unloaded quality factor from the following expression:

$$Q_u(f_0') = \frac{2\pi f_0' \Gamma}{R_s(f_0')} \approx \frac{2\pi f_{\rm I} \Gamma}{R_s(f_{\rm I})} = Q_u(f_{\rm I}) \tag{31}$$

where f_0' is the real part of the complex eigenfrequency reported by the solver, $R_s(f_0')$ is the surface resistance calculated at that frequency, given by (23) when neglecting the displacement current term, and Γ is the geometrical factor in

$$\Gamma = \mu_0 \frac{\int\int\int_v \boldsymbol{H} \cdot \boldsymbol{H}^* dV}{\int\int_s \boldsymbol{H}_t \cdot \boldsymbol{H}_t^* dS} \tag{32}$$

where V represents the internal volume of the cavity, S the internal surface area of the cavity walls and suffix "t" represents the field components tangential to the internal surface of the walls. This approach gives correct results for the unloaded quality factor $Q_u(f_{\rm I})$, since it takes into account the fields distribution and, thus, its accuracy is not significantly compromised by errors in the complex eigenfrequencies. However, the user needs to manually mesh the dielectric filler (e.g., air in this case) inside the cavity to make it dense enough so that the corresponding fields are captured accurately. Furthermore, for sufficiently high conductivities, f_0' (and, therefore, f_0) tends to $f_{\rm I}$, thus (31) approximately gives $Q_u(f_{\rm I})$; the percentage error of $|[Q_u(f_0) - Q_u(f_{\rm I})]/Q_u(f_{\rm I})| < 0.1\%$ is very small, which practically means that $Q_u(f_0) \cong Q_u(f_{\rm I})$ to a good approximation. Also, it should be noted that for faster convergence the box "*convergence on real frequency only*" must be ticked.

Although this latter approach produces accurate results for the unloaded Q-factor, it cannot provide accurate results for the frequency detuning and, thus, its use is limited to cases where only the ideal resonant frequency $f_{\rm I}$ and $Q_u(f_{\rm I})$ are of interest.

C. CST MWS

In contrast to HFSS™, with CST MWS, the walls of the cavity are assumed to be Perfect Electric Conductors (PEC), because its eigenmode solver does not support lossy metals; the unloaded quality factor can be extracted by entering the conductivity of the metal at the post-processing stage. It should be noted that a normal metal can be emulated by a dielectric material, but this still requires a high meshing density; making it impractical. However, CST MWS does not report the actual complex eigenfrequency of the cavity; only the ideal resonant frequency $f_{\rm I}$. The complex eigenfrequency $\tilde{f}_0$ can be calculated approximately using the general solution for lumped-element *RLC* resonators [36], but with the lossless resonant frequency f_0 and associated unloaded quality factor values $Q_u(f_0)$ replaced by those generated by CST MWS; more specifically

$$\tilde{f}_0 \sim f_{\rm I} \sqrt{1 - \left(\frac{1}{2Q_u(f_{\rm I})}\right)^2} + j\frac{f_{\rm I}}{2Q_u(f_{\rm I})}. \tag{33}$$

Not surprisingly, as can been seen in Fig. 3, this approach results in a significant error when predicting frequency detuning. Once again, only real conductivity values can be entered and so this approach can only be used for the simple relaxation-effect and classical skin-effect models.

D. EMPro and RSoft

With EMPro its eigenmode solver does not support frequency dispersive metals (this also applies to its FEM solver) and, thus, it cannot be used with either relaxation-effect models for arbitrary structures. However, in the unusually special case where the resonant frequency is known *a priori*, the surface impedance at the resonance can be entered (as with HFSS™), but this approach suffers from the same issues described previously.

Lastly, RSoft does not provide a 3D eigenmode solver and so the user has to excite the structure using its FullWave module, in frequency f_0'. The use of its finite-difference time-domain (FDTD) solver is beyond the scope of this study. Table I summarizes the modeling strategies for all the eigenmode solvers.

V. Spoof Surface Plasmon Waveguide Modeling

Spoof surface plasmons are a type of surface waves that are supported by a patterned metallic surface and widely modeled in various simulation domains [37]–[39]. Although a complete analysis is beyond the scope of this work, it will be shown using the available commercial frequency-domain software packages that there are differences in the simulation results. Our chosen benchmark structure has periodically spaced rectangular blind holes (i.e., open cavities) that do not completely perforate the metal film [40], as illustrated in Fig. 4. The width w and length l dimensions of the holes' aperture are 150 μm and 500 μm, respectively, with a periodicity d of 250 μm and depth h of either 100, 140, or 635 μm.

Fig. 5 shows a comparison for PEC structures using the results from [40], obtained by FDTD simulations, and corresponding HFSS™ simulations; while Fig. 6 shows a comparison of the experimental measured results from [40], obtained by taking the Fourier transform of time-domain measurements, and corresponding HFSS™ simulations using the FCB to model

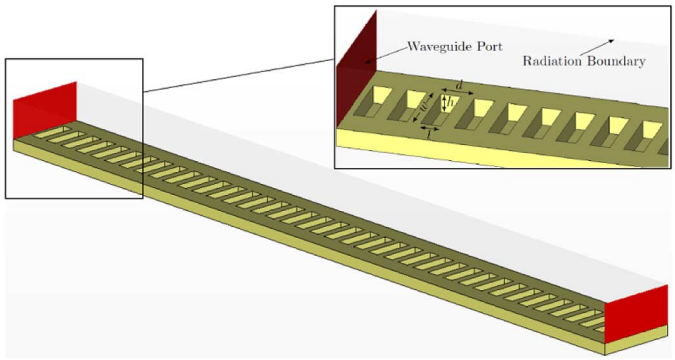

Fig. 4. Spoof surface plasmon waveguide benchmark structure with 40 blind holes, having a 10 mm total length.

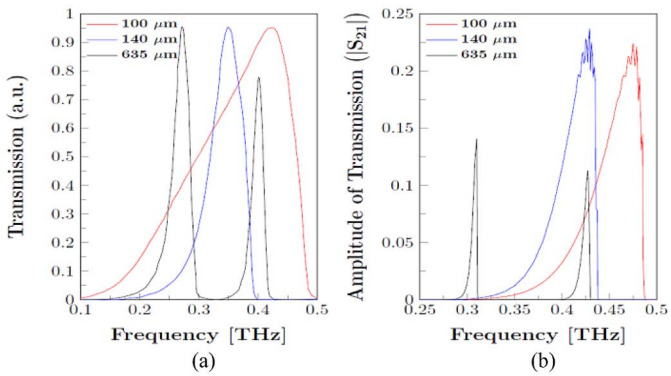

Fig. 5. Simulated transmission results for PEC structures with different blind hole depths from (a) Results in [40]; and (b) HFSS™.

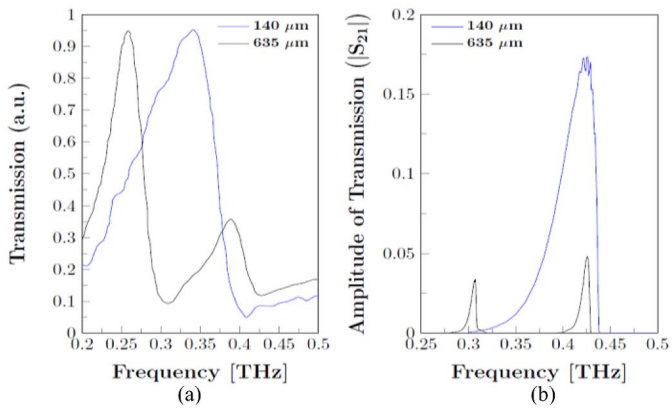

Fig. 6. Transmission results for aluminum structures from (a) Experimental results in [40]; and (b) FCB simulation results using HFSS™.

the fabricated aluminum structure. With $\sigma_0 = 3.767 \times 10^7$ S/m, $\tau = 7.407$ fs and $\mu_r' = 1.000021$ [22]; $\sigma'(f)$ was calculated for use with the simple relaxation-effect model.

It is seen in Figs. 5 and 6 that HFSS™ predicts a much sharper upper cut-off frequency response than the corresponding results given in [40], which in turn gives a slightly higher frequency for the peak in transmission. However, they do agree in that as depth increases the upper cut-off frequency of the dominant mode shifts down in frequency. The data presented also differs because transmission is calculated from the amplitude of the E-field component along the propagation direction in [40],

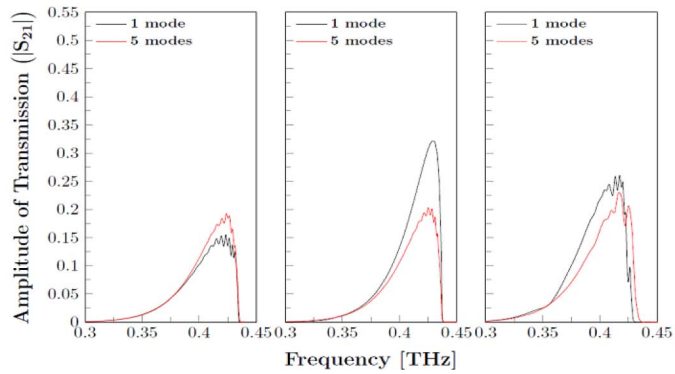

Fig. 7. Simulated transmission results of gold spoof surface plasmon waveguides for the dominant mode using: (left) HFSS™; (middle) CST MWS; (right) EMPro.

rather than by the S_{21} in HFSS™. In addition, from [40], the differences between their predicted and measured results shown in Figs. 5(a) and 6(a), respectively, is largely due to the introduction of the considerable ohmic losses (represented by the nonzero R_s) that degrades the slope of the cut-off frequencies and significant frequency detuning (represented by the nonzero X_s) that shifts the response down in frequency. In addition, there could be further detuning attributed to poor fabrication tolerances from the nonideal manufacturing process. It should be noted that the data presented in [40] has been normalized with scaling factors that are not specified in their paper; therefore, the HFSS™ results cannot be scaled to match those in [40].

Since HFSS™ modeling has been shown to behave as expected, CST MWS and EMPro were also used to simulate the structure in Fig. 4 having blind holes in a gold substrate.

The FCB boundary (or its equivalent) was used by all three software packages, as they were able to solve this problem in the frequency domain with waveguide excitations. RSoft was not considered for this more complicated 3D structure (i.e., having a nonuniform cross section, when compared to the MPRWG) because it would require the use of its time-domain solver, which is beyond the scope of this study.

The results are given in Fig. 7, showing that initial simulations with just the single dominant mode S_{21} provide widely varying predictions from each software package. Further simulations were then performed with the lowest five modes excited at the ports, but with the results extracted for the dominant mode S_{21}, as shown in Fig. 7. It can be seen that the software packages agree when more modes are included.

The large discrepancies found with the frequency-domain solver in CST MWS have been attributed to the complicated broadband frequency response of the structure and so the use of their transient solver was recommended [41].

Fig. 8 shows that there is little difference between the various boundaries and frequency dispersion models employed when 5 modes are excited at the ports and then the total transmission is calculated by the linear summation of all the 5 $|S_{21}|$ values for the dominant port mode. Since the maximum simulation frequency is only 0.45 THz, the results obtained with FCB (using the classical skin-effect model) are almost identical to those obtained with the LIB (using the classical relaxation-effect model); although this may not be the case when the dominant mode is at significantly higher frequencies. However, with

TABLE II
MATERIAL INPUT PARAMETERS FOR HFSS™

Material Type	Input Parameters			Comments for use with metal-based structures
	Relative permittivity $\boldsymbol{\varepsilon_r}$	Bulk conductivity $\boldsymbol{\sigma}$	Dielectric loss tangent $\boldsymbol{tan\delta}$	
General Case complex intrinsic permittivity complex intrinsic bulk conductivity	$\varepsilon'_{r,eff}(f)$	0	$\frac{\varepsilon''_{eff}(f)}{\varepsilon'_{eff}(f)}$	Excessive computational resources and processing time needed
Metal-like Case real intrinsic permittivity complex intrinsic bulk conductivity	$\varepsilon'_{r,eff}(f)$	$\sigma'(f)$	0	Ideal for classical relaxation-effect frequency dispersion model
Dielectric-like Case complex intrinsic permittivity real intrinsic bulk conductivity	$\varepsilon'_{r}(f)$	$\sigma'(f)$	$\frac{\varepsilon''(f)}{\varepsilon'(f)}$	Only valid for the simple relaxation-effect and classical skin-effect frequency dispersion models

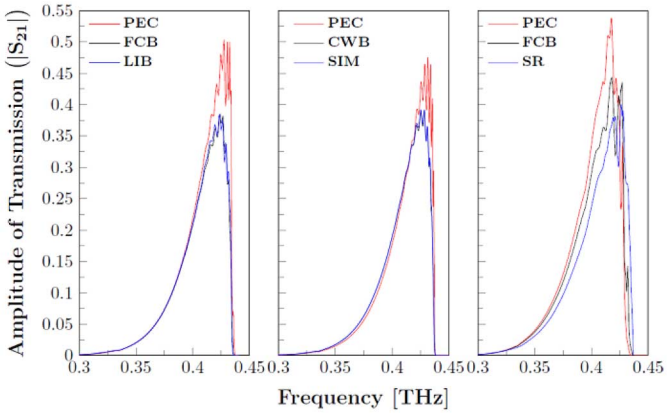

Fig. 8. Simulated transmission results for the spoof surface plasmon waveguide with five modes excited at the ports using: (left) HFSS™; (middle) CST MWS; (right) EMPro.

EMPro there is a notable difference in the predicted transmission heights and levels of detuning.

This section has highlighted the need for multiple-mode excitation, even if only the results for the dominant mode are needed. If the computational burden is not significantly increased, more modes should be calculated at the output for each excited port mode in order to achieve more accurate results.

VI. DISCUSSION

It has been shown that finding the correct modeling strategy is not always straightforward, when employing even well-known commercial EM solvers, for modeling metal-based THz structures. It is important to understand how the software code runs in the background and what input data it expects the user to enter. For example, in the HFSS™ Technical Notes (version 13) it is stated that permittivity can be complex and the effective permittivity is formulated as

$$\varepsilon_{\text{eff}} = \varepsilon_0 \boldsymbol{\varepsilon_r} \left(1 - j\mathbf{tan\delta} - j\frac{\boldsymbol{\sigma}}{\omega\varepsilon_0\boldsymbol{\varepsilon_r}}\right). \tag{34}$$

In order to avoid introducing further confusion, in this section, parameters in **bold font** correspond to input parameters in HFSS™ (rather than vectors, found in previous sections).

Now, it is not unambiguously stated that all input parameters must be real numbers, including relative permittivity $\boldsymbol{\varepsilon_r}$ and bulk conductivity $\boldsymbol{\sigma}$, in order for the code to calculate ε_{eff}, which is the only parameter needed by the solver. Unlike CST MWS, HFSS™ does not check for invalid input arguments (i.e., complex-valued parameters) and so no errors or warnings appear during setup or simulations. This can leave the user with a false sense of security, after the final results are reported by HFSS™. As can be seen in (34), the three input parameters are the relative permittivity $\boldsymbol{\varepsilon_r}$, the dielectric loss tangent $\mathbf{tan\delta}$ and the bulk conductivity $\boldsymbol{\sigma}$.

For the general case, where both the intrinsic relative permittivity and intrinsic bulk conductivity are represented by complex numbers (i.e., $\varepsilon(\omega) = \varepsilon'(\omega) - j\varepsilon''(\omega)$ and $\sigma(\omega) = \sigma'(\omega) - j\sigma''(\omega)$, respectively), the HFSS™ parameters that should be entered so that (34) is consistent with (12) are $\boldsymbol{\varepsilon_r} \rightarrow \varepsilon'_{r,\text{eff}}(\omega)$, $\mathbf{tan\delta} \rightarrow \varepsilon''_{\text{eff}}(\omega)/\varepsilon'_{\text{eff}}(\omega)$ and $\boldsymbol{\sigma} \rightarrow 0$; resulting in $\varepsilon_{\text{eff}}(\omega) = \varepsilon_o\varepsilon'_{r,\text{eff}}(\omega)\,(1 - j\varepsilon''_{\text{eff}}(\omega)/\varepsilon'_{\text{eff}}(\omega))$. However, because $\boldsymbol{\sigma} \rightarrow 0$, the "solve inside" function is automatically enabled. Therefore, this approach is impractical for metals, due to the excessive computational resources and processing time needed for the very high mesh densities associated with this function.

Alternatively, for the metal-like case, where a material is described by a real-value intrinsic permittivity and complex-value intrinsic bulk conductivity (e.g., metals with $\boldsymbol{\varepsilon_r} \cong 1$ and $\sigma(\omega) = \sigma'(\omega) - j\sigma''(\omega)$) the parameters $\boldsymbol{\varepsilon_r} \rightarrow \varepsilon'_{r,\text{eff}}(\omega)$, $\mathbf{tan\delta} \rightarrow 0$ and $\boldsymbol{\sigma} \rightarrow \sigma'(\omega)$ yield the correct results and (34) gives $\varepsilon_{\text{eff}}(\omega) = \varepsilon_o\varepsilon'_{r,\text{eff}}(\omega)\left(1 - j\sigma'(\omega)/\omega\varepsilon_o\varepsilon'_{r,\text{eff}}(\omega)\right)$. An example of this approach was used to simulate plasma-walled MPRWGs [42].

Similarly, for the dielectric-like case, where a material is described by complex-value intrinsic permittivity and real-value intrinsic bulk conductivity (e.g., dielectrics with $\varepsilon(\omega) = \varepsilon'(\omega) - j\varepsilon''(\omega)$ and $\sigma(\omega) = \sigma'(\omega)$) the HFSS™ parameters $\boldsymbol{\varepsilon_r} \rightarrow \varepsilon'_r$, $\mathbf{tan\delta} \rightarrow \varepsilon''(\omega)/\varepsilon'(\omega)$ and $\boldsymbol{\sigma} \rightarrow \sigma'(\omega)$ yield $\varepsilon_{\text{eff}}(\omega) = \varepsilon_o\varepsilon'_r(\omega)\,(1 - j\varepsilon''(\omega)/\varepsilon'(\omega) - j\sigma_o/\omega\varepsilon_o\varepsilon'_r(\omega))$. This is a valid approach, but only for the simple relaxation-effect and classical skin-effect models.

These three scenarios are summarized in Table II. The important message to note is that loose terminology leads to ambiguities and potentially significant errors. To the best of our knowledge, this is the first time that a clear and unambiguous description has been given for correctly entering material parameters for HFSS™.

For metal-based THz structures, instead of using solid metal objects, boundaries can be employed to avoid the problems related with the "solve inside" function. Macros can be used

by writing a Visual Basic Script (VBScript) to define various dispersion models for materials that can then be employed in a "solid object" or boundary. For example, the VBScript suggested by Ansys [35] calculates the material parameters based on Drude's classical relaxation-effect model, by entering the intrinsic bulk dc conductivity σ_o and the phenomenological scattering relaxation time τ. As with the general case, the calculated material parameters ($\boldsymbol{\varepsilon_r} \rightarrow \varepsilon'_{r,\mathrm{eff}}(\omega)$, $\mathbf{tan\delta} \rightarrow \varepsilon''_{\mathrm{eff}}(\omega)/\varepsilon'_{\mathrm{eff}}(\omega)$) are then used as input parameters for (34). However, as explained previously, this general-case modeling approach requires $\boldsymbol{\sigma} \rightarrow 0$ and, thus, the material created by the VBScript cannot be used with the FCB, LIB, or IB. As a result, the material can only be used to define "solid objects" with the "solve inside" function automatically enabled. Again, this approach does not give accurate results when metals-based structures are modeled, due to inadequate meshing inside the metal.

HFSS™ can generally give accurate results once the user has properly set up the simulation. Although this may seem trivial, the user has many more options (compared to the other software packages being investigated) to define materials but not all of them lead to correct solutions. However, HFSS™ is the only one (among the four frequency-domain software packages) that has a full 3D eigenmode solver capable of producing accurate and meaningful results.

On the other hand, in CST MWS and RSoft, it is straightforward to define the material parameters; the software automatically blocks the parameter fields that conflict with one other. In addition, once the input parameters are entered, their validity is checked, with error messages appearing in the case of an unexpected input.

VII. Conclusion

For the first time, an exhaustive comparative study has been made to investigate the use of well-known commercial frequency-domain solvers for the modeling of metal-based THz structures. Using the documentation provided by each of the four EM software package vendors, and in consultation with their technical support teams, various approaches to modeling benchmark metal-based THz structures have been studied. As suitable references, classical frequency dispersion models were applied to define material parameters. Since few measured results are available in the open literature for THz metal-pipe rectangular waveguides [22], or their associated cavities, only those for the spoof surface plasmon waveguide could be found using time-domain techniques to give a limited means of comparison [40].

While accurate verification measurements for this work are highly desirable, in practice it is believed that this very important task is not generally possible and so beyond the scope of this study. The reason for this is that NIST-traceable standards do not yet exist for frequency-domain metrology between 0.3 and 10 THz. Therefore, the corresponding measurement errors at such short wavelengths are likely to swamp those found in this numerical simulation study.

It has been found that the correct approach to selecting the most appropriate boundary conditions, defining a material's parameters and being able to enter its real or complex values within the software are not always straightforward. This paper highlights intuitive and logical approaches that give incorrect results and, where possible, makes recommendations for the most appropriate solutions that have hitherto not been given in Technical Notes.

This work has highlighted important weaknesses in well-known commercial frequency-domain EM modeling software packages currently being used for THz simulations. It is hoped that existing software vendors will be able to address these issues, by revising Technical Notes with unambiguous user-input material parameter definitions (with all necessary caveats) and/or ideally upgrading the software. With the latter, there may be significant reluctance by vendors, due to the costs associated with further software development.

While the use of time-domain solvers has been beyond the scope of this work, the authors believe that similar challenges to obtaining accurate results will be found.

It is believed that this paper gives, for the first time, a detailed comparative insight into the most appropriate use of commercial frequency-domain EM solvers for the numerical simulation of arbitrary metal-based THz structures. As a result, newcomers to the field of numerical EM simulators, as well as experienced designers, will be able to predict the performance of passive metal-based THz components with more confidence in the generated results.

Finally, the findings presented in this paper could act as a benchmark for the comparison and development of existing and future numerical simulation software intended for THz applications. However, while it is hoped that this study will encourage the development of more accurate frequency-domain solvers and help engineers and scientists design more accurate THz structures, it also raises fundamental questions on the *laissez faire* use of commercial EM software packages as an effective validation tool in the absence of accurate measurements.

Acknowledgment

One of the authors, Dr. S. Lucyszyn, would like to acknowledge Prof. M. Kuwata-Gonokami, at the Photon Science Center of the University of Tokyo, for hosting some of this work. The authors would like to thank the technical support teams from the various software vendors, for their valuable suggestions and discussions—(HFSS™: Dr. D. Edgar; CST: Dr. M. Rütschlin and Till Steiner; RSoft: J. Horgan and M. Frank; and EMPro: A. Perez and H. Spiegel).

References

[1] H. Kazemi, S. T. Wootton, N. J. Cronin, S. R. Davies, R. E. Miles, R. D. Pollard, J. M. Chamberlain, D. P. Steenson, and J. W. Bowen, "Active micromachined integrated terahertz circuits," *Int. J. Infrared Millim. Waves*, vol. 20, no. 5, pp. 967–974, Mar. 1999.

[2] F. Maiwald, S. Martin, J. Bruston, A. Maestrini, T. Crawford, and P. H. Siegel, "2.7 THz waveguide tripler using monolithic membrane diodes," in *IEEE MTT-S Int. Microw. Symp. Dig.*, May 2001, vol. 3, pp. 1637–1640.

[3] J. W. Bowen, S. Hadjiloucas, B. M. Towlson, L. S. Karayzas, S. T. G. Wootton, N. J. Cronin, S. R. Davies, C. E. McIntosh, J. M. Chamberlain, R. E. Miles, and R. D. Pollard, "Micromachined waveguide antennas for 1.6 THz," *Electron. Lett.*, vol. 42, no. 15, pp. 842–843, Jul. 2006.

[4] A. Pavolotsky, D. Meledin, C. Risacher, M. Pantaleev, and V. Belitsky, "Micromachining approach in fabricating of THz waveguide components," *Microelectron. J.*, vol. 36, pp. 683–686, Jun. 2005.

[5] C. D. Nordquist, M. C. Wanke, A. M. Rowen, C. L. Arrington, M. Lee, and A. D. Grine, "Design, fabrication, and characterization of metal micromachined rectangular waveguides at 3 THz," in *Int. Symp. on Antennas and Propag. Soc. (AP-S 2008)*, Jul. 2008, pp. 1–4.
[6] T. H. Hand, Y. Yuan, S. Palit, C. Bingham, M. Rahm, D. R. Smith, W. J. Padilla, N. Jokerst, and S. A. Cummer, "Dual-band planar electric THz metamaterial with resonator yield analysis," in *2008 Conf. on Lasers and Electro-Optics and 2008 Conf. on Quantum Electron. and Laser Sci. (CLEO/QELS 2008)*, May 2008, pp. 1–2.
[7] N. Llombart and P. H. Siegel, "Cylindrically periodic dielectric waveguide at submillimeter waves," in *2008 IEEE Int. Symp. on Antennas Propag. Soc. (AP-S 2008)*, Jul. 2008, pp. 1–4.
[8] W. Miao, Y. Delorme, F. Dauplay, G. Beaudin, Q. J. Yao, and S. C. Shi, "Simulation of an integrated log-spiral antenna at terahertz," in *Int. Symp. on Antennas, Propag. and EM Theory (ISAPE 2008)*, Nov. 2008, pp. 58–61.
[9] K. R. Jha, S. V. R. K. Rao, and G. Singh, "Constructive interference in Yagi-Uda type printed terahertz antenna on photonic crystal substrate," in *IEEE Sarnoff Symp.*, Apr. 2010, pp. 1–5.
[10] M. Theuer, C. Imhof, G. Torosyan, F. Ellrich, R. Zengerle, and R. Beigang, "Pump beam diameter dependent terahertz generation from surface emitters—Experiment and simulation," in *Int. Conf. on Infrared, Millim. THz Waves (IRMMW-THz 2008)*, Sep. 2008, pp. 1–2.
[11] K. R. Jha and G. Singh, "Analysis of dielectric permittivity and losses of two-layer substrate materials for microstrip antenna at THz frequency," in *Int. Conf. on Adv. in Recent Technologies in Commun. and Comput, (ARTCom '09)*, Oct. 2009, pp. 672–675.
[12] C. J. Lin, C. H. Lin, Y. T. Li, R. P. Pan, and C. L. Pan, "Electrically controlled liquid crystal phase grating for terahertz waves," *IEEE Photon. Technol. Lett.*, vol. 21, no. 11, pp. 730–732, Jun. 2009.
[13] F. Zhan, G. Qiaoqiang, Y. J. Ding, and F. J. Bartoli, "From waveguiding to spatial localization of THz waves within a plasmonic metallic grating," *IEEE J. Sel. Topics Quantum Electron.*, vol. 14, no. 2, pp. 486–490, Mar. 2008.
[14] B. Y. Shew, H. C. Li, C. L. Pan, and C. H. Ko, "X-ray micromachining SU-8 resist for a terahertz photonic filter," *J. Phys. D: Appl. Phys.*, vol. 38, no. 7, pp. 1097–1103, Mar. 2005.
[15] G. Qiaoqiang and F. J. Bartoli, "Graded metallic gratings for ultrawideband surface wave trapping at THz frequencies," *IEEE J. Sel. Topics Quantum Electron.*, vol. 17, no. 1, pp. 102–109, Jan. 2011.
[16] D. Sanchez-Escuderos, M. Ferrando-Bataller, M. Baquero-Escudero, and J. I. Herranz, "Ebg structures for antenna design at THz frequencies," in *IEEE Int. Symp. on Antennas Propag. (APSURSI)*, Jul. 2011, pp. 1824–1827.
[17] P. Peier, H. Merbold, V. Pahinin, K. A. Nelson, and T. Feurer, "Imaging of THz waves in 2D photonic crystals structures embedded in a slab waveguide," *New J. Phys.*, vol. 12, p. 013014, Jan. 2010.
[18] E. Episkopou, S. Papantonis, W. J. Otter, and S. Lucyszyn, "Demystifying material parameters for terahertz electromagnetic simulation," in *4th U.K./Eur.-China Conf. on Millim. Waves and THz Technol.*, Sep. 2011, pp. 80–81.
[19] J. Y. Choi and S. Lucyszyn, "HFSS™ modelling anomalies with electrically thin-walled metal-pipe rectangular waveguide simulations," in *10th IEEE High Freq. Postgraduate Student Colloq.Dig.*, Leeds, U.K., Sep. 2005, pp. 95–98.
[20] Y. Zhou and S. Lucyszyn, "HFSS™ modelling anomalies with thz metal-pipe rectangular waveguide structures at room temperature," *PIERS Online J.*, vol. 5, no. 3, pp. 201–211, 2009.
[21] J. Hoffmann, C. Hafner, P. Leidenberger, J. Hesselbarth, and S. Burger, "Comparison of electromagnetic field solvers for the 3D analysis of plasmonic nano antennas," *Proc. SPIE 7390, 73901G*, Feb. 2010.
[22] S. Lucyszyn, "Investigation of anomalous room temperature conduction losses in normal metals at terahertz frequencies," *IEE Proc. Microw., Antennas Propag.* , vol. 151, no. 4, pp. 321–329, Aug. 2004.
[23] S. Lucyszyn, "Investigation of Wang's model for room temperature conduction losses in normal metals at terahertz frequencies," *IEEE Trans. Microw. Theory Techn.*, vol. 53, no. 4, pp. 1398–1403, Apr. 2005.
[24] S. Lucyszyn and Y. Zhou, "Engineering approach to modelling frequency dispersion within normal metals at room temperature for THz applications," *PIER J.*, vol. 101, pp. 257–275, Feb. 2010.
[25] C. P. Smyth, *Dielectric Behavior and Structure: Dielectric Constant and Loss, Dipole Moment, and Molecular Structure*, 1st ed. New York: McGraw-Hill, 1955.
[26] F. A. Grant, "Use of complex conductivity in the representation of dielectric phenomena," *J. Appl. Phys.*, vol. 29, no. 1, pp. 76–80, Jan. 1958.
[27] K. L. Ngai and R. W. Rendell, "Interpreting the real part of the dielectric permittivity contributed by mobile ions in ionically conducting materials," *Phys. Rev. B*, vol. 61, no. 14, Apr. 2000.
[28] T. W. Kim, W. P. Beyermann, D. Reagor, and G. Gruner, "Complex conductivity measurements at several frequencies in the millimetre wave spectral range," *Rev. Sci. Instrum.*, vol. 59, no. 7, Jul. 1988.
[29] U. Kaatze, "Complex permittivity of water as a function of frequency and temperature," *J. Chem. Eng. Data*, vol. 34, no. 4, pp. 371–374, Oct. 1989.
[30] S. Lucyszyn, "Microwave characterization of nickel," *PIERS Online J.*, vol. 4, no. 6, pp. 686–690, Jun. 2008.
[31] S. Lucyszyn and Y. Zhou, "THz applications for the engineering approach to modelling frequency dispersion within normal metals at room temperature," *PIERS Online J.*, vol. 6, no. 3, pp. 293–299, Feb. 2010.
[32] Int. Org. for Standardization (ISO), Geneva, Switzerland, "Guide to the choice of series of preferred numbers and of series containing more rounded values of preferred numbers," ISO 497:1973, 1973 [Online]. Available: http://www.iso.org/iso/iso_catalogue/catalogue_tc/catalogue_detail.htm?csnumber=4548
[33] R. E. Collin, *Field Theory of Guide Waves*, 1st ed. New York: Wiley-IEEE Press, 1991, pp. 340–354.
[34] S. Lucyszyn, D. Budimir, Q. H. Wang, and I. D. Robertson, "Design of compact monolithic dielectric-filled metal-pipe rectangular waveguides for millimetre-wave applications," *IEE Proc. Microw., Antennas and Propag.*, vol. 143, no. 5, pp. 451–453, Oct. 1996.
[35] D. Edgar, Ansys Corporation, Nov. 2010, private communication.
[36] J. C. Slater, "Microwave electronics," *Rev. Modern Phys.*, vol. 18, no. 4, pp. 441–512, Oct. 1946.
[37] Z. Yu, G. Veronis, S. Fan, and M. L. Brongersma, "Design of midinfrared photodetectors enhanced by surface plasmons on grating structures," *Appl. Phys. Lett.*, vol. 89, no. 15, Oct. 2006.
[38] B. K. Juluri, S. S. Lin, T. R. Walker, L. Jensen, and T. J. Huang, "Propagation of designer surface plasmons in structured conductor surfaces with parabolic gradient index," *Opt. Express*, no. 17, pp. 2997–3006, Feb. 2009.
[39] S. A. Maier, S. R. Andrews, L. Martin-Moreno, and F. J. Garcia-Vidal, "Terahertz surface plasmon-polariton propagation and focusing on periodically corrugated metal wires," *Phys. Rev. Lett.*, vol. 97, p. 176805, Oct. 2006.
[40] G. Kumar, S. Pandey, A. Cui, and A. Nahata, "Planar plasmonic terahertz waveguides based on periodically corrugated metal films," *New J. Phys.*, vol. 13, p. 033024, Mar. 2011.
[41] M. Rütschlin, CST, 2012, private communication.
[42] Y. Zhou and S. Lucyszyn, "Modelling of reconfigurable terahertz integrated architecture (RETINA) SIW structures," *PIER J.*, vol. 105, pp. 71–92, Jun. 2010.

Elpida Episkopou (S'11) was born in Athens, Greece, in 1986. She received the Dipl.-Ing. degree in electrical and computer engineering from the University of Patras, Greece, in 2010, and is currently working toward the Ph.D. degree from Imperial College London, London, U.K.

Her main research interests include hybrid opto-electromagnetic terahertz structures.

Stergios Papantonis (S'11) was born in Hannover, Germany, in 1986. He received the Dipl.-Ing. degree in electrical and computer engineering, from the University of Patras, Greece, in 2010, and is currently working toward the Ph.D. degree from Imperial College London, London, U.K.

His main research interests are in the areas of metamaterials and electromagnetic wave propagation.

William James Otter (S'12) received the M.Eng. degree in electrical and electronic engineering from Imperial College London, London, U.K., in 2010. During this period he undertook industrial placements at BAE Systems, Advanced Technology Centre, Great Baddow, U.K. He is currently working toward the Ph.D. degree from Imperial College London.

His current research interests include terahertz filter design and material modeling. He holds the Val O'Donoghue Scholarship in the Department of Electrical and Electronic Engineering.

Stepan Lucyszyn (M'91–SM'04) received the Ph.D. degree in electronic engineering from King's College London (University of London), U.K., and the D.Sc. (higher doctorate) degree in millimeter-wave and terahertz electronics from Imperial College London, London, U.K., in 1992 and 2010, respectively.

He is currently a Reader (Associate Professor) in Millimeter-wave Electronics and the Director of the Centre for Terahertz Science and Engineering, Imperial College London. After working in industry, as a satellite systems engineer for maritime and military communications, he spent the first 12 years researching microwave and millimeter-wave RFIC/MMICs, followed by RF MEMS technologies. For over 15 years, he has been working on millimeter-wave electronics and, since 2004, investigating the behavior of materials, passive structures and ubiquitous applications at THz frequencies. Between 2010 and 2011, he spent one year at the Photon Science Center, University of Tokyo, Japan, within the Gonokami Laboratory (Department of Physics). He has (co)-authored approximately 135 papers and 11 book chapters in applied physics and electronic engineering, and delivered many invited presentations at international conferences.

From 2005 to 2009, Dr. Lucyszyn served as an Associate Editor for the IEEE/ASME JOURNAL OF MICROELECTROMECHANICAL SYSTEMS. In 2011, he was the Chairman of the 41st European Microwave Conference, held in Manchester, U.K. In 2005, he was elected Fellow of the Institution of Electrical Engineers, U.K., and Fellow of the Institute of Physics, U.K., and in 2008 was invited as a Fellow of the Electromagnetics Academy, USA. In 2009 he was appointed an IEEE Distinguished Microwave Lecturer for 2010–2012.